Research Article Vol. 10, No. 7 / July 2023 / Optica 841

Full control of electric and magnetic light–matter interactions through a nanomirror on a near-field tip

Benoît Reynier,[1] Eric Charron,[1] Obren Markovic,[1] Xingyu Yang,[1] Bruno Gallas,[1] Alban Ferrier,[2,3] Sébastien Bidault,[4] and Mathieu Mivelle[1,*]

[1]Sorbonne Université, Centre National de la Recherche Scientifique, Institut des NanoSciences de Paris, 75005 Paris, France
[2]Chimie ParisTech, Paris Sciences & Lettres University, Centre National de la Recherche Scientifique, Institut de Recherche de Chimie Paris, 75005 Paris, France
[3]Faculté des Sciences et Ingénierie, Sorbonne Universités, UFR 933, 75005 Paris, France
[4]Institut Langevin, ESPCI Paris, Université PSL, CNRS, 75005 Paris, France
*mathieu.mivelle@sorbonne-universite.fr

Received 23 January 2023; revised 2 May 2023; accepted 3 May 2023; published 28 June 2023

Light–matter interactions are often considered governed by the electric optical field only, leaving aside the magnetic component of light. However, the magnetic part plays a determining role in many optical processes, from light and chiral-matter interactions and photon-avalanching to forbidden photochemistry, making the manipulation of magnetic processes extremely relevant. Here, by creating a standing wave using a metallic nanomirror, we manipulate the spatial distributions of electric and magnetic fields and their associated local densities of states, allowing selective control of the excitation and emission of electric and magnetic dipolar transitions. This control allows us to image, in 3D, the electric and magnetic nodes and anti-nodes of the fields' interference patterns. It also enables us to enhance specifically photoluminescence from quantum emitters excited only by the magnetic field, and to manipulate their spontaneous emission by acting on the excitation fields solely, demonstrating full control of magnetic and electric light–matter interactions.

https://doi.org/10.1364/OPTICA.486207

1. INTRODUCTION

Manipulating light–matter interactions at the nanoscale has revolutionized many scientific fields, whether in biology, with ever more sensitive diagnostics platforms [1,2], medicine with targeted therapies [3,4], chemistry with higher efficiency catalysis [5,6], or physical optics with ever more exotic manipulations of these interactions [7–11]. Nevertheless, most of the systems developed to date have aimed at manipulating the electric component of light, leaving aside its magnetic counterpart. Indeed, light–matter interactions are often considered driven by the electric optical field alone, ignoring the magnetic component of light. However, this magnetic component plays a key role in many optical processes, such as chiral light–matter interactions [12], ultrasensitive detection [13], enhancement of Raman optical activity [14], photon-avalanching [15], or forbidden photochemistry [16], which makes the manipulation of magnetic processes extremely important. Over the past few years, several studies have demonstrated a manipulation of specific "magnetic light"–matter interactions. For instance, luminescence mediated by magnetic transition dipoles was controlled and enhanced by manipulating the magnetic local density of states (LDOS) through metallic layers acting as mirrors [17–22] or with resonant dielectric [23–32] and plasmonic [33–36] nanostructures. It was also demonstrated that a Bessel beam could selectively excite a magnetic dipole transition through the magnetic field of light [37].

Here, we introduce a new platform made of a metallic nanomirror creating a standing wave pattern to manipulate the spatial distributions of electric and magnetic fields and the associated LDOSs. With this platform, we demonstrate the selective excitation of electric (ED) or magnetic (MD) dipolar transitions and selectively collect the luminescence emitted by ED or MD transitions. This control allows us to image, in 3D, the electric and magnetic nodes and anti-nodes of the fields' interference patterns. It also allows us to specifically enhance the luminescence of the quantum emitter by magnetic excitation only and to manipulate the spontaneous emission of the particle by acting on the excitation fields only, thus demonstrating total control of magnetic and electric light–matter interactions.

2. RESULTS

For this purpose, a metallic nano-antenna is fabricated at the tip of an aluminum-coated tapered optical fiber (see Supplement 1) in a scanning near-field optical microscope (SNOM) and acts as a nanomirror when excited from the far field to create a standing wave (Fig. 1). This electromagnetic field is used to excite a Eu^{3+}-doped Y_2O_3 nanoparticle (see Supplement 1), whose position can be scanned at the nanoscale in 3D under the SNOM tip, allowing dynamic control of the interactions.

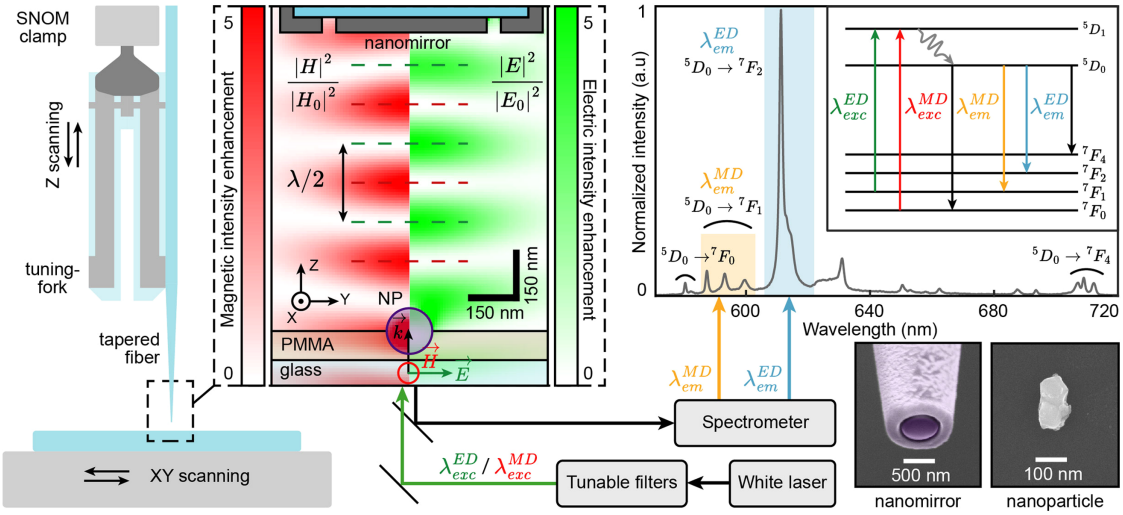

Fig. 1. Principle of the experiment. A metallic nanomirror fabricated at the tip of a tapered fiber and placed on a SNOM (see Supplement 1) is brought near a Y_2O_3 nanoparticle (NP) doped with Eu^{3+} ions. The excitation is performed by a spectrally tunable laser, and the luminescence signal is collected using a spectrometer. Numerical simulations of the standing wave generated by the metallic nanomirror are displayed. The interferences of the magnetic intensity of the standing wave at λ_{exc}^{MD} are on the left side, in red, and those of the electric intensity at λ_{exc}^{ED} on the right side, in green. Both intensities are normalized by the amplitude of the incident field. The dotted lines are guides for the eye showing the spatial separation of the electric and magnetic anti-nodes in the standing wave. The purple circle indicates the Eu^{3+}-doped particle. The emission spectrum (for excitation at $\lambda_{exc}^{ED} = 532$ nm) of Eu^{3+} ions in the Y_2O_3 matrix, with the magnetic and electric transitions of interest highlighted, respectively, in yellow and blue, is represented (see Supplement 1 for the emission spectrum when the particles are excited through the magnetic transition at $\lambda_{exc}^{MD} = 527.5$ nm). The partial band diagram of Eu^{3+} ions shows the electric (λ_{exc}^{ED}) and magnetic (λ_{exc}^{MD}) transitions at the excitation and, respectively, at the emission (λ_{em}^{ED}, λ_{em}^{MD}).

Eu^{3+} ions are known to exhibit pure electric and magnetic transitions in the visible spectrum, in terms of both excitation [37] and emission [18] (partial band diagram in the inset of Fig. 1). The excitation of ED (at $\lambda_{exc}^{ED} = 532$ nm) and MD (at $\lambda_{exc}^{MD} = 527.5$ nm) transitions is then performed by a white laser coupled to series of tunable filters, allowing the reduction of the laser spectrum to a bandwidth of only 2 nm. This bandwidth was chosen to minimize the cross talk between electric and magnetic excitations according to the excitation spectrum of Eu^{3+} ions (see Fig. S1 in Supplement 1). The luminescence of the ED (at $\lambda_{em}^{ED} = 610$ nm) and MD (at $\lambda_{em}^{MD} = 590$ nm) transitions of the Eu^{3+} ions is then collected by the same objective, filtered from the laser light, and measured by a spectrometer. The emission spectrum of europium ions is shown in Fig. 1. By tuning the position of the nanoparticle within the standing wave, we can thus selectively excite it with the E or H field and selectively collect the signal emitted by ED and MD transitions. Therefore, we have access to the 3D distributions of the electromagnetic fields and of the local densities of optical states that act on the quantum emitters (i.e., Eu^{3+}).

Figure 1 shows the theoretical spatial distributions (see Supplement 1) of the electric and magnetic fields generated by the standing wave beneath the metallic nanomirror at λ_{exc}^{ED} and λ_{exc}^{MD} wavelengths, respectively. We observe that the electric and magnetic nodes and anti-nodes do not overlap spatially. A maximum E field corresponds to a minimum H field and vice versa. Furthermore, inside the anti-nodes, the field intensities are increased by a factor of five compared to the incident wave. Finally, due to the different continuity conditions at the interfaces, we can see that the two components of light do not penetrate the doped nanoparticle in the same way, with a clear predominance of the magnetic field inside the latter. Interestingly, this means that E and H excitations take place at slightly different positions within the nanoparticle, as detailed further in the following paragraphs. Note that the amplitudes of the maxima of the electric and magnetic fields are due to the contributions of the reflection on the mirror, the gap between the nanodisc and the aluminum on the surface of the tip, the presence of the substrate, and the increase of the field within the particle. In particular, the presence of the particle and the substrate influences the amplitude of the standing wave but not the position of its nodes and anti-nodes (see paragraph 2 of Supplement 1 for the field maps of these different conditions).

The luminescence intensity L of the europium-doped nanoparticle is proportional to the average excitation intensity within the nanoparticle according to the following equation: $L = \sigma |A|^2 \eta Q$, where σ is the absorption cross section, A is the electric or magnetic excitation field, η is the collection efficiency, and Q is the quantum yield. Figure 2(a) provides the luminescence collected at λ_{em}^{ED} when exciting the particle at λ_{exc}^{ED} and λ_{exc}^{MD} for different antenna–particle distances Z and normalized with respect to the luminescence intensities without the nanomirror. We observe that the signals do not overlap spatially: the maxima and minima for these two excitations are almost inversed, in excellent agreement with the theoretical results expected from the excitation of the particle by the E or H field of light (see paragraph 2 of Supplement 1 for different particle geometries). These measurements thus indicate that the evolution of L as a function of Z follows directly the evolution of the excitation probability and that Q and η have a negligible influence on the spatial distributions of luminescence intensities. Importantly, since Q and η are independent of the nature of the excitation process (MD or ED) and depend only on Z, it is possible to divide the luminescence enhancement measured at λ_{exc}^{ED} by the luminescence enhancement measured at λ_{exc}^{MD} and recover directly the ratio between the intensity enhancements of the E and H fields, providing a quantitative agreement between measurements and theory (see Fig. S2 in Supplement 1). These results also indicate that there is no spectral cross talk between the

two excitation channels, although, it should be noted that even if Q and η do not influence the spatial distributions of the E and H fields, the difference in contrast between the theoretical and experimental curves in Figs. 2(a) and 2(b) can be explained by the fact that the experimental results, i.e., the number of photons collected, depend of the quantum yield of the dipoles and the collection efficiency of our system. These quantities are not considered in the theoretical results of Figs. 2(a) and 2(b), which represent only the contributions of the electric and magnetic fields within the particle. Moreover, the shapes of the particles can also influence this contrast (paragraph 2 of the Supplement 1).

As a control experiment, the measurement is also performed using a 200 nm diameter nanoparticle filled with fluorescent molecules [Fig. 2(b); see Supplement 1]. In this case, magnetic transitions are negligible compared to their electrical counterparts, and the absorption spectrum overlaps with both λ_{exc}^{ED} and λ_{exc}^{MD} wavelengths (see Fig. S1 in Supplement 1). For fluorescent nanospheres, the curves are perfectly superimposed, and the signal follows a purely electric excitation. This measurement confirms that the luminescence collected in Fig. 2(a) for a λ_{exc}^{ED} excitation represents the spatial distribution of the E field intensity in the standing wave and that the signal for a λ_{exc}^{MD} excitation maps the magnetic field. Furthermore, we observe that the fluorescence intensity is enhanced by a factor of three and 2.5 for, respectively, the excitation by E and H fields compared to the signal collected without the antenna. This measurement provides the first demonstration of an enhanced luminescence signal from quantum emitters excited specifically by the magnetic component of light.

Moreover, using the SNOM nano-positioning capabilities, the luminescence of Eu^{3+} ions collected for each particle position in the volume under the nanomirror provides a 3D spatial reconstruction of the E and H field intensities of the standing wave as shown in Fig. 2(c). Here, the E and H nodes and anti-nodes are observed as lobes of the standing wave because of the nanoscale size of the metallic mirror. This is the first 3D image providing, in parallel, the intensities of the electric and magnetic components of light.

Finally, by tuning the excitation wavelength and studying separately the ED and MD emission intensities, we study how the metallic nanomirror modifies the spontaneous emission rates for an electric or magnetic excitation. Since the emitted photons originate from the same excited state, we can infer the β^{ED} and β^{MD} branching ratios by considering any other transitions and non-radiative decay channels as losses [20]:

$$\beta^{ED} = \frac{L^{ED}}{L^{ED} + L^{MD}} = 1 - \beta^{MD}, \quad (1)$$

where L^{ED} and L^{MD} are, respectively, the luminescence signal emitted by electric and magnetic transitions.

It is then possible to determine the relative LDOSs experienced by ED (at λ_{em}^{ED}) and MD (at λ_{em}^{MD}) transitions as [20]

$$\rho^{ED} = \frac{\rho^{ED}}{\rho^{ED} + \rho^{MD}} = \frac{\beta_{NM}^{ED}/\beta_0^{ED}}{\beta_{NM}^{ED}/\beta_0^{ED} + \beta_{NM}^{MD}/\beta_0^{MD}} = 1 - \rho^{MD}, \quad (2)$$

with β_{NM} and β_0 representing the branching ratios with and without a nanomirror, respectively. Figure 3 provides the radiative electric LDOS when exciting the particle using the E or H field, for different nanomirror–particle distances. Interestingly, these two LDOSs, although measured at the same positions and thus in the same photonic environment, do not overlap spatially. The explanation can be found in the non-finite size of the

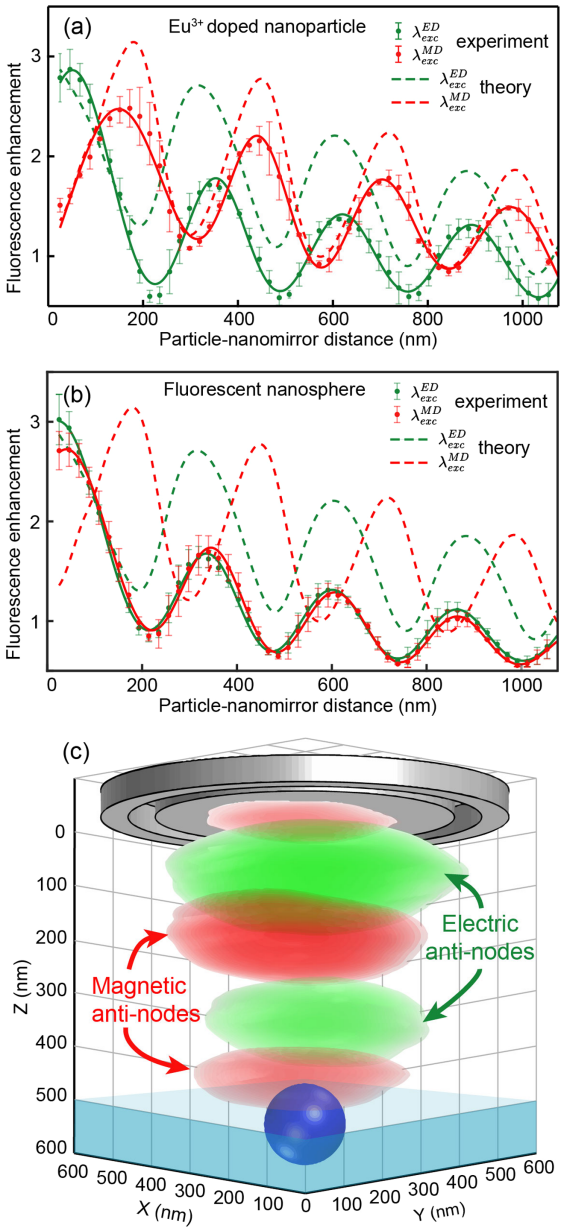

Fig. 2. Optical characterization of the standing wave. (a) Increase of the luminescence intensities emitted by the Eu^{3+}-doped particle and collected by the spectrometer for excitation wavelengths at λ_{exc}^{ED} (green) and λ_{exc}^{MD} (red) and for different Z positions of the particle under the nanomirror. (b) Increase in fluorescence intensity emitted from nanospheres filled with fluorescent molecules (see Supplement 1) for different Z positions under the nanomirror and excited at λ_{exc}^{ED} (green) and λ_{exc}^{MD} (red). In (a) and (b), points correspond to the average values of experimental data normalized by the signal without the antenna, solid curves are polynomial fits serving as guides for the eye, and dashed curves correspond to numerical calculations of the expected signal for an excitation by the magnetic field (red) or the electric field (green) of light. The error bars correspond to the standard deviation. (c) 3D image of the electric (green) and magnetic (red) nodes and anti-nodes of the electromagnetic standing wave generated under the nanomirror.

Eu^{3+}-doped nanoparticle. Indeed, depending on the component of light that interacts with the particle, the position of the excited ions will not spatially overlap because of a different spatial distribution of the fields within the particle as shown in Figs. 3(e)–3(j)

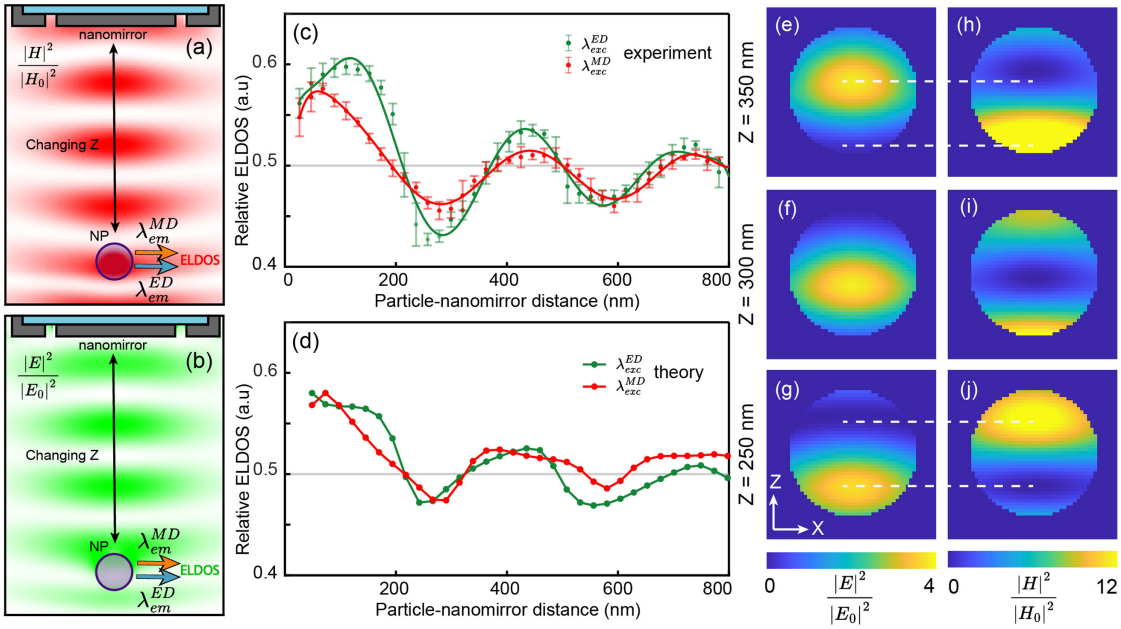

Fig. 3. LDOS change through field excitation. Principle of the experiment. The nanoparticle is excited by (a) the magnetic field (at $\lambda_{exc}^{MD} = 527.5$ nm) or (b) the electric field (at $\lambda_{exc}^{ED} = 532$ nm) for different mirror–particle distances. For each position, the number of photons emitted through the electric (at $\lambda_{em}^{ED} = 610$ nm) and magnetic (at $\lambda_{em}^{MD} = 590$ nm) channels are collected and used to calculate the relative electric LDOS (ELDOS) via Eqs. (1) and (2). (c) Experimental and (d) theoretical relative electric LDOSs as a function of the particle–nanomirror distance when the Eu^{3+} ions are excited at the resonance wavelength of the magnetic dipole transition (red) or the electric dipole transition (green). In (c), solid curves are polynomial fits serving as guides for the eye, and the error bars correspond to the standard deviation; $Z = 0$ is chosen as the top part of the doped particle. Theoretical distribution of (e)–(j) electric (at λ_{exc}^{ED}) and (f)–(h) magnetic (at λ_{exc}^{MD}) optical fields inside the nanoparticle, normalized by the incident wave and for different Z positions of the particle under the nanomirror (indicated on the left side). A mask is applied to remove the fields outside of the particle for clarity, and the diameter of the nanoparticle is 150 nm.

(see paragraph 2 of Supplement 1 for different particle geometries). The emitting ions will therefore be at different positions corresponding to a different LDOS. Thus, by changing the nature of the exciting field, it is possible to turn on or off some ions and probe different spatial distributions of the LDOSs for electric and magnetic transition dipoles. These subtle variations are in good agreement with theoretical calculations when the LDOS, inferred from the photoluminescence measurements, is balanced by the distribution of the excitation fields within the particle [Figs. 3(e)–3(j)].

3. CONCLUSION

In conclusion, through a new platform, we demonstrated that by generating a standing wave with a nanomirror at the end of a SNOM tip, we could perfectly control the electric and magnetic interactions of light with quantum emitters, in terms of both the excitation probability and spontaneous decay channels. This manipulation allowed us to provide the first experimental 3D image of the electric and magnetic nodes and anti-nodes of a standing wave. Furthermore, we demonstrated an increase in the emission of a quantum emitter after specific excitation of its magnetic transition dipole, and we showed how, by this full control of the interactions, we could, in particular, manipulate the spontaneous emission of an emitter only by acting on the nature (magnetic or electric) of its excitation. This research opens the way to many photonic applications involving a contribution from the optical magnetic field, such as chiral light–matter interactions [12], photochemistry [16], manipulation of magnetic processes [38], and new schemes in quantum computing [39] or nonlinear processes [15], among others.

Funding. China Scholarship Council; Agence Nationale de la Recherche (ANR-20-CE09-0031-01, ANR-22-CE09-0027-04); Institut de physique (Tremplin@INP 2020).

Acknowledgment. M.M. supervised the study. B.R., E.C., and O.M. performed the experiments. B.R. and X.Y. performed the numerical study. A.F. synthesized the Eu^{3+}-doped nanoparticles. B.R., B.G., S.B., and M.M. analyzed the data. All authors discussed the results and contributed to writing the manuscript.

Disclosures. The authors declare no conflicts of interest.

Data availability. The data underlying the results presented in this paper are not publicly available at this time but may be obtained from the authors upon reasonable request.

Supplemental document. See Supplement 1 for supporting content.

REFERENCES

1. D. Punj, M. Mivelle, S. B. Moparthi, T. S. van Zanten, H. Rigneault, N. F. van Hulst, M. F. García-Parajó, and J. Wenger, "A plasmonic 'antenna-in-box' platform for enhanced single-molecule analysis at micromolar concentrations," Nat. Nanotechnol. **8**, 512–516 (2013).
2. P. M. Winkler, R. Regmi, and V. Flauraud, "Antenna-based fluorescence correlation spectroscopy to probe the nanoscale dynamics of biological membranes," Nano Lett. **9**, 110–119 (2018).
3. D. P. O'Neal, L. R. Hirsch, N. J. Halas, J. D. Payne, and J. L. West, "Photo-thermal tumor ablation in mice using near infrared-absorbing nanoparticles," Cancer Lett. **209**, 171–176 (2004).
4. P. Fortina, L. J. Kricka, D. J. Graves, J. Park, T. Hyslop, F. Tam, N. Halas, S. Surrey, and S. A. Waldman, "Applications of nanoparticles to diagnostics and therapeutics in colorectal cancer," Trends Biotechnol. **25**, 145–152 (2007).

5. R. Grisel, K.-J. Weststrate, A. Gluhoi, and B. E. Nieuwenhuys, "Catalysis by gold nanoparticles," Gold Bull. **35**, 39–45 (2002).
6. R. Sardar, A. M. Funston, P. Mulvaney, and R. W. Murray, "Gold nanoparticles: past, present, and future," Langmuir **25**, 13840–13851 (2009).
7. T. Taminiau, F. Stefani, F. Segerink, and N. Van Hulst, "Optical antennas direct single-molecule emission," Nat. Photonics **2**, 234–237 (2008).
8. M. L. Juan, M. Righini, and R. Quidant, "Plasmon nano-optical tweezers," Nat. Photonics **5**, 349–356 (2011).
9. D. Akinwande, C. Huyghebaert, C.-H. Wang, M. I. Serna, S. Goossens, L.-J. Li, H.-S. P. Wong, and F. H. Koppens, "Graphene and two-dimensional materials for silicon technology," Nature **573**, 507–518 (2019).
10. J. J. Baumberg, J. Aizpurua, M. H. Mikkelsen, and D. R. Smith, "Extreme nanophotonics from ultrathin metallic gaps," Nat. Mater. **18**, 668–678 (2019).
11. B. Yang, G. Chen, A. Ghafoor, Y. Zhang, Y. Zhang, Y. Zhang, Y. Luo, J. Yang, V. Sandoghdar, and J. Aizpurua, "Sub-nanometre resolution in single-molecule photoluminescence imaging," Nat. Photonics **14**, 693–699 (2020).
12. Y. Tang and A. E. Cohen, "Optical chirality and its interaction with matter," Phys. Rev. Lett. **104**, 163901 (2010).
13. Z. Xi and H. Urbach, "Magnetic dipole scattering from metallic nanowire for ultrasensitive deflection sensing," Phys. Rev. Lett. **119**, 053902 (2017).
14. T. Wu, X. Zhang, R. Wang, and X. Zhang, "Strongly enhanced Raman optical activity in molecules by magnetic response of nanoparticles," J. Phys. Chem. C **120**, 14795–14804 (2016).
15. C. Lee, E. Z. Xu, Y. Liu, A. Teitelboim, K. Yao, A. Fernandez-Bravo, A. M. Kotulska, S. H. Nam, Y. D. Suh, and A. Bednarkiewicz, "Giant nonlinear optical responses from photon-avalanching nanoparticles," Nature **589**, 230–235 (2021).
16. A. Manjavacas, R. Fenollosa, I. Rodriguez, M. C. Jiménez, M. A. Miranda, and F. Meseguer, "Magnetic light and forbidden photochemistry: the case of singlet oxygen," J. Mater. Chem. C **5**, 11824–11831 (2017).
17. N. Noginova, Y. Barnakov, H. Li, and M. Noginov, "Effect of metallic surface on electric dipole and magnetic dipole emission transitions in Eu^{3+} doped polymeric film," Opt. Express **17**, 10767–10772 (2009).
18. S. Karaveli and R. Zia, "Spectral tuning by selective enhancement of electric and magnetic dipole emission," Phys. Rev. Lett. **106**, 193004 (2011).
19. T. H. Taminiau, S. Karaveli, N. F. van Hulst, and R. Zia, "Quantifying the magnetic nature of light emission," Nat. Commun. **3**, 979 (2012).
20. L. Aigouy, A. Cazé, P. Gredin, M. Mortier, and R. Carminati, "Mapping and quantifying electric and magnetic dipole luminescence at the nanoscale," Phys. Rev. Lett. **113**, 076101 (2014).
21. R. Hussain, S. S. Kruk, C. E. Bonner, M. A. Noginov, I. Staude, Y. S. Kivshar, N. Noginova, and D. N. Neshev, "Enhancing Eu^{3+} magnetic dipole emission by resonant plasmonic nanostructures," Opt. Lett. **40**, 1659–1662 (2015).
22. F. T. Rabouw, P. T. Prins, and D. J. Norris, "Europium-doped $NaYF_4$ nanocrystals as probes for the electric and magnetic local density of optical states throughout the visible spectral range," Nano Lett. **16**, 7254–7260 (2016).
23. B. Rolly, B. Bebey, S. Bidault, B. Stout, and N. Bonod, "Promoting magnetic dipolar transition in trivalent lanthanide ions with lossless Mie resonances," Phys. Rev. B **85**, 245432 (2012).
24. T. Feng, Y. Xu, Z. Liang, and W. Zhang, "All-dielectric hollow nanodisk for tailoring magnetic dipole emission," Opt. Lett. **41**, 5011–5014 (2016).
25. D. G. Baranov, R. S. Savelev, S. V. Li, A. E. Krasnok, and A. Alù, "Modifying magnetic dipole spontaneous emission with nanophotonic structures," Laser Photon. Rev. **11**, 1600268 (2017).
26. T. Feng, W. Zhang, Z. Liang, Y. Xu, and A. E. Miroshnichenko, "Isotropic magnetic Purcell effect," ACS Photon. **5**, 678–683 (2017).
27. M. Sanz-Paz, C. Ernandes, J. U. Esparza, G. W. Burr, N. F. van Hulst, A. Maitre, L. Aigouy, T. Gacoin, N. Bonod, M. F. Garcia-Parajo, S. Bidault, and M. Mivelle, "Enhancing magnetic light emission with all-dielectric optical nanoantennas," Nano Lett. **18**, 3481–3487 (2018).
28. A. Vaskin, S. Mashhadi, M. Steinert, K. E. Chong, D. Keene, S. Nanz, A. Abass, E. Rusak, D.-Y. Choi, I. Fernandez-Corbaton, T. Pertsch, C. Rockstuhl, M. A. Noginov, Y. S. Kivshar, D. N. Neshev, N. Noginova, and I. Staude, "Manipulation of magnetic dipole emission from Eu^{3+} with Mie-resonant dielectric metasurfaces," Nano Lett. **19**, 1015–1022 (2019).
29. P. R. Wiecha, C. Majorel, C. Girard, A. Arbouet, B. Masenelli, O. Boisron, A. Lecestre, G. Larrieu, V. Paillard, and A. Cuche, "Enhancement of electric and magnetic dipole transition of rare-earth-doped thin films tailored by high-index dielectric nanostructures," Appl. Opt. **58**, 1682–1690 (2019).
30. X. Cheng, X. Zhuo, R. Jiang, Z. G. Wang, J. Wang, and H. Q. Lin, "Electromagnetic resonance-modulated magnetic emission in europium-doped sub-micrometer zirconia spheres," Adv. Opt. Mater. **9**, 2002212 (2021).
31. H. Sugimoto and M. Fujii, "Magnetic Purcell enhancement by magnetic quadrupole resonance of dielectric nanosphere antenna," ACS Photon. **8**, 1794–1800 (2021).
32. Y. Brûlé, P. Wiecha, A. Cuche, V. Paillard, and G. C. des Francs, "Magnetic and electric Purcell factor control through geometry optimization of high index dielectric nanostructures," Opt. Express **30**, 20360–20372 (2022).
33. S. M. Hein and H. Giessen, "Tailoring magnetic dipole emission with plasmonic split-ring resonators," Phys. Rev. Lett. **111**, 026803 (2013).
34. M. Mivelle, T. Grosjean, G. W. Burr, U. C. Fischer, and M. F. Garcia-Parajo, "Strong modification of magnetic dipole emission through diabolo nanoantennas," ACS Photon. **2**, 1071–1076 (2015).
35. B. Choi, M. Iwanaga, Y. Sugimoto, K. Sakoda, and H. T. Miyazaki, "Selective plasmonic enhancement of electric-and magnetic-dipole radiations of Er ions," Nano Lett. **16**, 5191–5196 (2016).
36. C. Ernandes, H.-J. Lin, M. Mortier, P. Gredin, M. Mivelle, and L. Aigouy, "Exploring the magnetic and electric side of light through plasmonic nanocavities," Nano Lett. **18**, 5098–5103 (2018).
37. M. Kasperczyk, S. Person, D. Ananias, L. D. Carlos, and L. Novotny, "Excitation of magnetic dipole transitions at optical frequencies," Phys. Rev. Lett. **114**, 163903 (2015).
38. D. Bossini, V. I. Belotelov, A. K. Zvezdin, A. N. Kalish, and A. V. Kimel, "Magnetoplasmonics and femtosecond optomagnetism at the nanoscale," ACS Photon. **3**, 1385–1400 (2016).
39. D. Serrano, S. K. Kuppusamy, B. Heinrich, O. Fuhr, D. Hunger, M. Ruben, and P. Goldner, "Ultra-narrow optical linewidths in rare-earth molecular crystals," Nature **603**, 241–246 (2022).